



Article

Employing PCBDTPP as an Efficient Donor Polymer for High Performance Ternary Polymer Solar Cells

Binrui Xu ^{1,†} , Gopalan Saianand ^{2,†} , V. A. L. Roy ³, Qiquan Qiao ⁴, Khan Mamun Reza ⁴ and Shin-Won Kang ^{1,*}

¹ School of Electronics Engineering, College of IT Engineering, Kyungpook National University, Daegu 41566, Korea

² Global Innovative Center for Advanced Nanomaterials, School of Engineering, Faculty of Engineering and Built Environment, The University of Newcastle, Callaghan, NSW 2308, Australia

³ Department of Materials Science and Engineering, City University of Hong Kong, Tat Chee Avenue, Kowloon 999077, Hong Kong, China

⁴ Department of Electrical Engineering and Computer Science, South Dakota State University, Brookings, SD 570007, USA

* Correspondence: swkang@knu.ac.kr; Tel.: +82-053-950-6829

† Authors contributed equally to this work.

Received: 21 August 2019; Accepted: 28 August 2019; Published: 29 August 2019



Abstract: A compatible low-bandgap donor polymer (poly[*N*-90-heptadecan-2,7-carbazole-alt-3,6-bis(thiophen-5-yl)-2,5-dioctyl-2,5-dihydropyrrolo[3,4]pyrrole-1,4-dione], PCBDTPP) was judiciously introduced into the archetypal poly(3-hexylthiophene):[6,6]-phenyl-C₆₁-butyric acid methyl ester (P3HT:PC₆₁BM) photoactive system to fabricate highly efficient ternary based bulk heterojunction polymer solar cells (PSCs). The PCBDTPP ternary-based PSC with optimal loading (0.2 wt.%) displayed outstanding performance with a champion power conversion efficiency (PCE) of 5.28% as compared to the PCE (4.67%) for P3HT:PC₆₁BM-based PSC (reference). The improved PCE for PCBDTPP ternary-based PSC can be mainly attributed to the incorporation of PCBDTPP into P3HT:PC₆₁BM that beneficially improved the optical, morphological, electronic, and photovoltaic (PV) performance. This work instills a rational strategy for identifying components (donor/acceptor (D/A) molecules) with complementary beneficial properties toward fabricating efficient ternary PSCs.

Keywords: polymer solar cells; low-bandgap; ternary; PCBDTPP

1. Introduction

Recently, polymer solar cells (PSCs) have triggered stupendous attention owing to their cost-competitiveness, mechanical flexibility, lightweight nature, and compatibility for large area deposition [1–7]. One of the most widely used donor/acceptor (D/A) photoactive blend systems is poly(3-hexylthiophene):[6,6]-phenyl-C₆₁-butyric acid methyl ester (P3HT:PC₆₁BM) [8–12]. So far, the power conversion efficiency (PCE) of PSCs with the conventional P3HT:PC₆₁BM system have achieved 3–5% [13–16]. However, further development on P3HT:PC₆₁BM-based PSCs is highly warranted to overcome the low short-circuit current density (J_{sc}), which can be improved by tailoring the relatively narrow absorption range due to the wide-bandgap nature of the P3HT. To widen the light absorption capability of the P3HT:PC₆₁BM and to further improve photovoltaic (PV) performance, numerous strategies have been widely demonstrated, such as synthesizing new low-bandgap materials, employing tandem PSCs, doping suitable D/A molecules, etc. [17–21]. Among them, adopting ternary-based PSCs can be considered one of the most promising strategies to manipulate/fine-tune the PV performance parameters of the PSCs [22,23]. Recently, a ternary photoactive blend system

(D/D/A, D/A/A) featuring a low-bandgap material with broad absorption spectra has been realized as a potential strategy to improve optical absorption, optimize the exciton separation, and charge carrier extraction in active layer with an aim of enhancing the J_{sc} and other performance parameters of PSCs [24–27]. Herein, we explored a new kind of unexplored low-bandgap polymer, poly[*N*-9-hepta-decanyl-2,7-carbazole-alt-3,6-bis-(thiophen-5-yl)-2,5-dioctyl-2,5-dihydropyrrolo[3,4]pyrrole-1,4-dione] (PCBTDP, Figure 1a), as an efficient donor into P3HT:PC₆₁BM active system to construct high-efficiency ternary PV devices with the device architecture (Figure 1b): indium tin oxide (ITO) glass/poly (3,4-ethylene dioxythiophene): poly (styrene sulfonate) (PEDOT:PSS)/binary or ternary photoactive blend system/Al. Figure 1c depicts the energy level bands of components involved, and their energy levels are derived from the relevant reports [28–31].

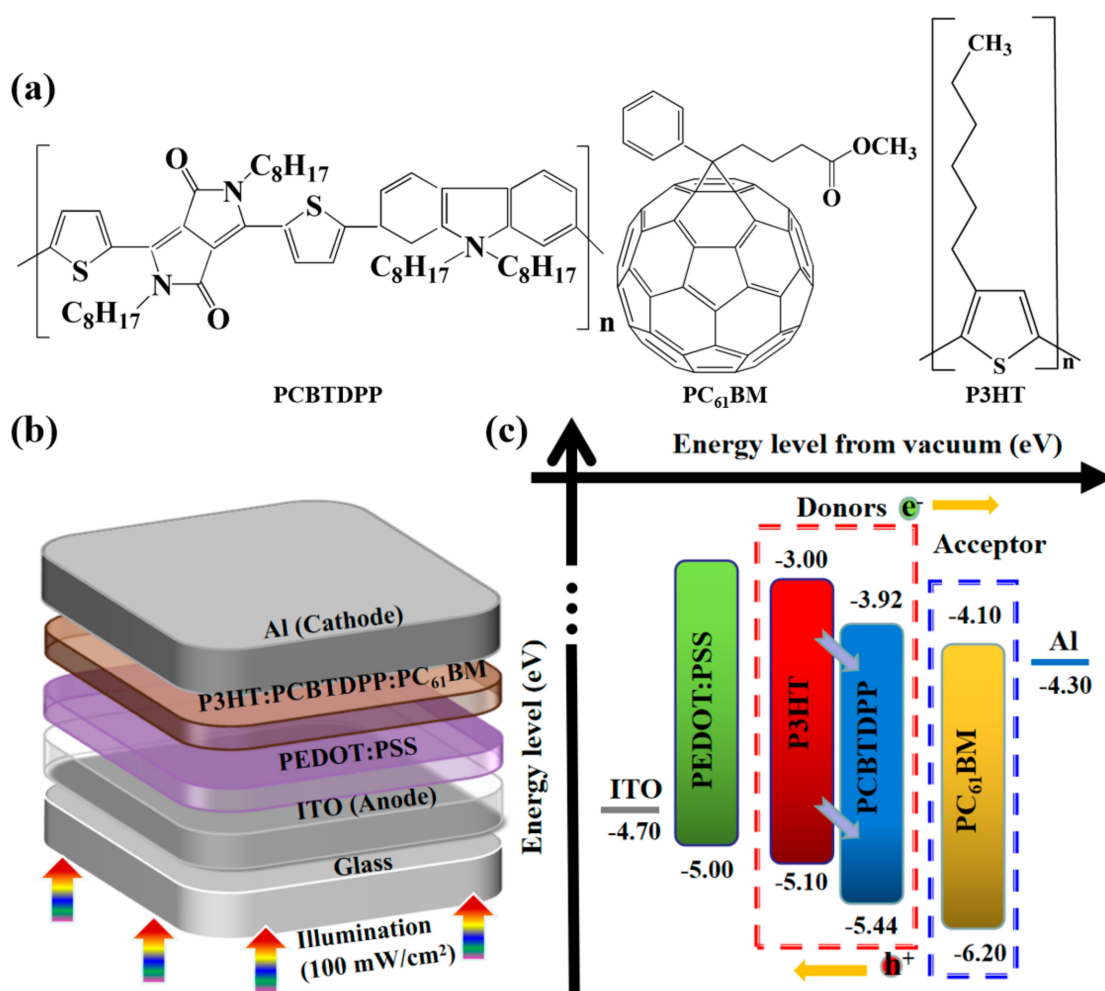


Figure 1. (a) The chemical structures of poly[*N*-90-heptadecanyl-2,7-carbazole-alt-3,6-bis(thiophen-5-yl)-2,5-dioctyl-2,5-dihydropyrrolo[3,4]pyrrole-1,4-dione] (PCBTDP), poly(3-hexylthiophene):[6,6] (P3HT), and phenyl-C₆₁-butyric acid methyl ester (PC₆₁BM), (b) device geometry, and (c) energy band levels of the studied components. ITO = indium tin oxide; poly (3,4-ethylene dioxythiophene): poly (styrene sulfonate) = PEDOT:PSS.

PCBTDP was primarily chosen for two main reasons. Firstly, PCBTDP is a low-bandgap (1.52 eV) donor with good stability, high mobility and complementary absorption spectrum (300–800 nm) to P3HT [29]. In addition, the highest occupied molecular orbital (HOMO) and the lowest unoccupied molecular orbital (LUMO) energy levels of PCBTDP are comparable to that of P3HT and PC₆₁BM. Secondly, PCBTDP has good compatibility and solubility in the photoactive blend, P3HT:PC₆₁BM (1,2-dichlorobenzene (DCB)), which is expected to influence the optoelectronic properties of the

ternary-based PSC. Earlier it was reported that PCBTDDP:PC₇₀BM based PSC witnessed an inferior PCE of 1.6% [32]. The beneficial optoelectronic properties of PCBTDDP in P3HT:PC₆₁BM based ternary PSC has not been harnessed so far. To the best of our knowledge, the role and influence of PCBTDDP into P3HT:PC₆₁BM on the optical, structural, morphology and PV performance has not been studied in detail. Hence, in this contribution, we clarify the relevant improvements on the optoelectronic properties, as well as their corresponding PV performance. Consequently, the ternary PSC-based on optimal loading of PCBTDDP (0.2 wt.%) into P3HT:PC₆₁BM witnessed a high PCE of 5.28%, while the fabricated binary P3HT:PC₆₁BM-based PSC only displayed a PCE of 4.67%.

2. Experimental

2.1. Materials

P3HT and PC₆₁BM were sourced from Lumtec, Taipei Taiwan, China. PCBTDDP and DCB were bought from Sigma-Aldrich, Seoul, Korea. Low conductive PEDOT:PSS (AI 4083) and highly conductive PEDOT:PSS (PH 500) were obtained from Baytron, H.C. Starck, Newton, MA, USA.

2.2. Photoactive Ink Formulation

P3HT, PCBTDDP and PC₆₁BM were blended together in host solvent, DCB with a varied weight ratio of PCBTDDP (0 to 0.3%), and stirred at 60 °C overnight. The weight ratio of PCBTDDP was chosen based on the weight ratio of P3HT.

2.3. Fabrication of PSCs

The ITO glass substrates (3 cm × 3 cm) were washed by acetone, methanol, and 2-propanol and UV ozone cured for 30 min based on our previous works [33–35]. Then, the prepared ITO glasses were dried by nitrogen gun and heated at 150 °C for 10 min. Two variants (low and highly conductive) of PEDOT:PSS (AI 4083 and PH 500) were independently deposited on the ITO glasses at 4000 rpm for 30 s and baked at 150 °C for 10 min, respectively. The as-prepared photoactive ink solution was spun onto PEDOT:PSS layer at 1200 rpm for 60 s. To complete the device fabrication, an Al electrode was thermally evaporated in high vacuum (1.5×10^{-5} Torr) to form an active area of 9 mm².

2.4. Characterization

The photocurrent density-voltage (*J-V*) parameters were recorded using a 2400 source meter (Keithley, Seoul, Korea) under solar simulator (XES-300S1, SAN-EI Electric Corporation, Osaka, Japan) with 100 mW/cm² (AM 1.5G). Ultraviolet-visible (UV-vis) absorption was collected a UV-vis spectrometer (Shimadzu Corporation, Kyoto, Japan), and photoluminescence (PL) spectra were measured by a PL spectrophotometer (Spectra pro 2150i, Acton Research Corporation, Greer, MA, USA). The morphological properties of active layers were recorded by an Agilent 5500 atomic force microscope (AFM) (Agilent Technologies, Santa Clara, CA, USA). The external quantum efficiency (EQE) data was examined by a lock-in amplifier (Newport Corporation, Irvine, CA, USA).

3. Results and Discussion

Figure 2a showed the UV-vis absorbance of as-deposited P3HT:PC₆₁BM and P3HT:PCBTDDP(0.2 wt.%) :PC₆₁BM active layers. Figure 2b showed the UV-vis absorbance of as-casted P3HT and PCBTDDP thin films, along with their respective PL spectrum of P3HT. The P3HT:PCBTDDP(0.2 wt.%) :PC₆₁BM film exhibited significantly improved absorption potential in the broadband range with high intensity, which is attributed to the complementary absorption spectra capability of PCBTDDP film (Figure 2b) [36,37]. PCBTDDP displayed strong light-absorbing ability from 615 nm to 700 nm, and the main absorption peaks of PCBTDDP was centered at 681 nm. Especially, the broaden absorption range between 720 nm and 800 nm in P3HT:PCBTDDP(0.2 wt.%) :PC₆₁BM blend system implied that the lower energy photons could be absorbed by PCBTDDP. It is believed that

good photon harvesting and efficient charge collection are the primary factors that help to enhance J_{sc} . Results from Figure 2b indicated that the PCBTDP absorption range covered the PL spectrum of P3HT, and could result in Förster resonance energy transfer (FRET) between P3HT and PCBTDP [38]. The exciton generated in P3HT or PCBTDP can be either dissociated at the D/A interfaces or directly transferred from P3HT to PCBTDP via FRET before dissociation [39]. The HOMO and LUMO energy levels of P3HT are -5.10 eV and -3.00 eV, while PCBTDP shows the HOMO of -5.44 eV and LUMO of -3.92 eV. The differences between LUMO levels of P3HT/PCBTDP and LUMO of PC₆₁BM are 1.10 eV and 0.18 eV, respectively, which can provide improved exciton dissociation and enhanced charge transport in P3HT:PCBTDP(0.2 wt.):PC₆₁BM layer. Herein, the energy level of PCBTDP was ideally placed in conjunction with P3HT and PC₆₁BM for a broadened absorption potential and enhanced charge carrier transport. Additionally, the PL (Figure 2c) for two active layers was acquired under 550 nm light excitation. The peak of P3HT PL intensity at ~ 552 nm was considerably quenched in P3HT:PCBTDP(0.2 wt.):PC₆₁BM as compared to P3HT:PC₆₁BM, suggesting an effective exciton dissociation in the fabricated ternary blend system [40].

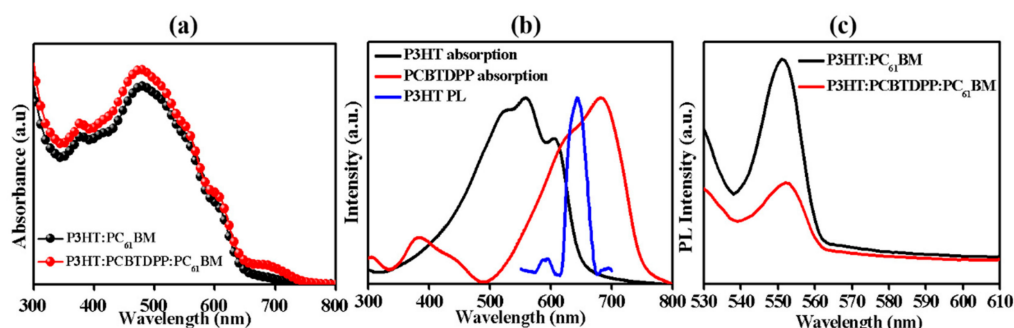


Figure 2. (a) UV-vis absorption of P3HT:PC₆₁BM and P3HT:PCBTDP(0.2 wt.):PC₆₁BM, (b) normalized absorption of as-casted P3HT and PCBTDP and the PL of the P3HT, and (c) PL of P3HT:PC₆₁BM and P3HT:PCBTDP(0.2 wt.):PC₆₁BM thin films.

The morphological aspects of the active blend system highly influence the performance of the PV device. To probe the morphological aspects of P3HT:PC₆₁BM and P3HT:PCBTDP(0.2 wt.):PC₆₁BM, tapping mode AFM images ($5 \mu\text{m} \times 5 \mu\text{m}$) were recorded and displayed in Figure 3a,b. Desirable nanoscale phase separation with uniform coverage and fiber-like structure (P3HT chains) with an excellent bicontinuous interpenetrating network were clearly observed for P3HT:PCBTDP(0.2 wt.):PC₆₁BM film, resulting from effective exciton dissociation, improved charge transport and reduced charge recombination [41,42]. The root mean square (RMS) roughness of binary and ternary active layers are 0.711 nm and 1.004 nm, respectively. The rougher ternary active layer could provide a larger interface contact between the P3HT:PCBTDP(0.2 wt.):PC₆₁BM film and Al, benefitting charge collection as well as a rapid pathway for charge transport, which leads to the quenching of PL response [43]. In addition, the rougher morphology might also induce stronger internal reflection, thus enhancing light absorbance of the active blend system. The change in RMS values indicated that the doping of PCBTDP into P3HT:PC₆₁BM allowed modification of the miscibility of P3HT and PC₆₁BM [44,45].

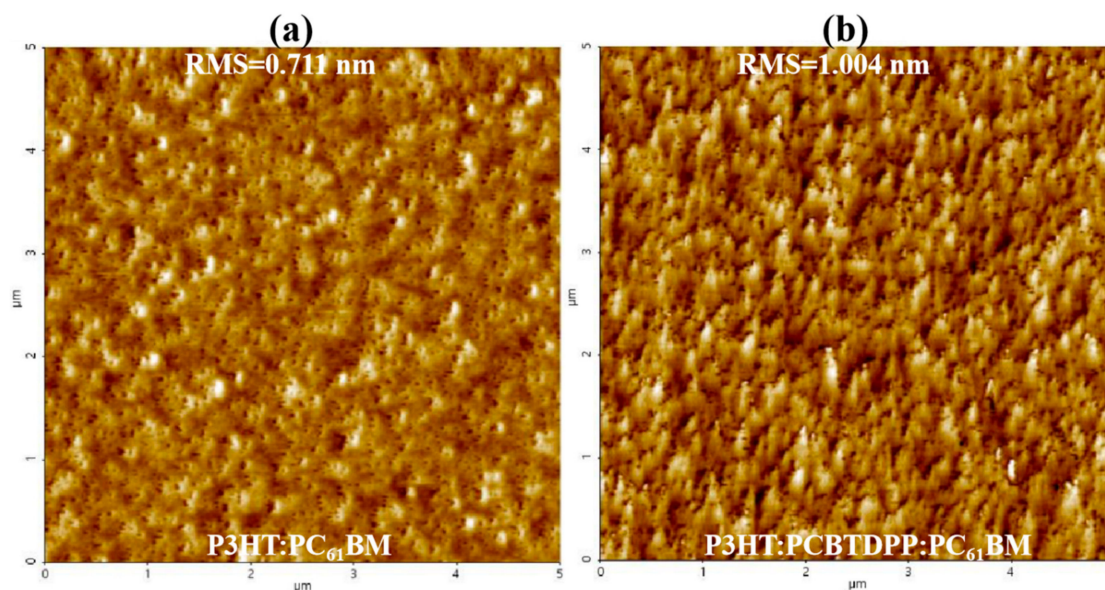


Figure 3. Atomic force microscope (AFM) topography images of the (a) binary and (b) ternary blend active layer coated atop ITO.

The J - V characteristics and corresponding PV performance parameters of the binary (P3HT:PC₆₁BM) and ternary (P3HT:PCBDTDP(0.2 wt.%):PC₆₁BM) based PSCs were shown in Figure 4a,b, Tables 1 and 2, respectively. By utilizing PEDOT:PSS (AI 4083) as a hole transport layer (HTL), the binary device showed a low PCE of 1.75%. On the contrary, the ternary P3HT:PCBDTDP(0.2 wt.%):PC₆₁BM based device achieved the PCE of 2.09%. With the aim of improving the device performance, we utilized PEDOT:PSS (PH 500) with 5% DMSO as HTL, the ternary PSCs achieved champion PCE of 5.28% with a high J_{sc} of 16.15 mA/cm², while the PCE and J_{sc} of the binary device were 4.67% and 14.75 mA/cm², respectively [46]. The high J_{sc} obtained in this work may be possibly due to doping of DMSO into PEDOT:PSS (PH 500) which would improve the conductivity of the PEDOT:PSS layer significantly. The increased PCE is also attributed to the enhanced J_{sc} , which arises from the enhanced optical absorption, modified morphology, and improved exciton dissociation through the judicious inclusion of PCBDTDP in the ternary active system. In order to investigate the absorption efficiency and charge carriers' dynamics, EQE spectra were recorded and shown in Figure 4c. Compared with the P3HT:PC₆₁BM (binary) based device, the P3HT:PCBDTDP(0.2 wt.%):PC₆₁BM (ternary) device exhibited improved EQE spectrum in a broad wavelength range (590~800 nm). In light of the optical properties, the EQE improvement mainly originates from the increased photon harvesting and the efficient exciton migration by FRET [47].

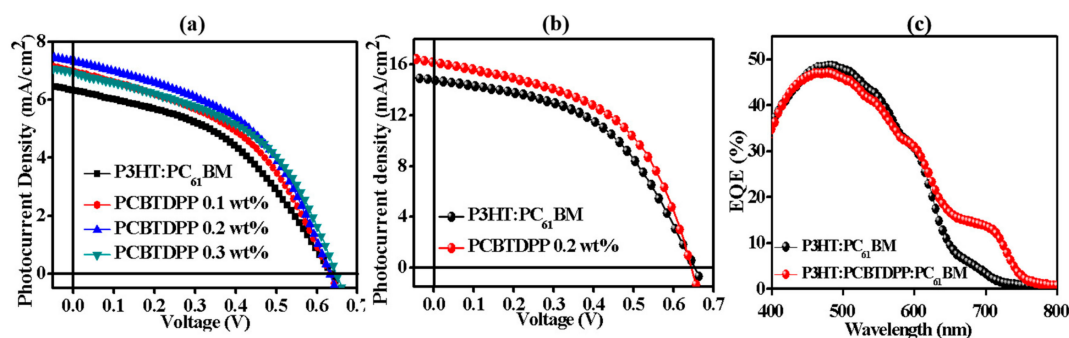


Figure 4. J - V curves of the devices based on (a) PEDOT:PSS (AI 4083) and (b) PEDOT:PSS (PH 500) with 5% DMSO and (c) EQE profiles of the devices based on P3HT:PC₆₁BM and P3HT:PCBDTDP(0.2 wt.%):PC₆₁BM.

Table 1. Summary of photovoltaic (PV) performances of the devices based on low conductive PEDOT:PSS (AI 4083).

PEDOT:PSS (AI 4083)	V_{oc} (V)	J_{sc} (mA/cm ²)	FF	PCE (%)
P3HT:PC ₆₁ BM	0.63	6.32	0.43	1.75
PCBTDPDP 0.1 wt.%	0.63	6.71	0.44	1.86
PCBTDPDP 0.2 wt.%	0.63	6.94	0.46	2.09
PCBTDPDP 0.3 wt.%	0.63	6.81	0.45	1.98

Table 2. Summary of PV performances of the devices based on highly conductive PEDOT:PSS (PH 500) with 5% DMSO.

PEDOT:PSS (PH 500)	V_{oc} (V)	J_{sc} (mA/cm ²)	FF	PCE (%)
P3HT:PC ₆₁ BM	0.65	14.75	0.48	4.67
PCBTDPDP 0.2 wt.%	0.64	16.15	0.50	5.28

Additionally, in order to highlight the functionality of PCBTDPDP in the ternary PSCs, we compared with some recent ternary PSCs based on the P3HT:PCBM:X (X: active component, D or A) (Table 3). In comparison with the previous reports, our ternary PSC-based on P3HT:PCBTDPDP(0.2 wt.):PC₆₁BM achieved the best PCE of 5.28%. This comparison clearly indicates that introducing PCBTDPDP into P3HT:PC₆₁BM active system is one of the most efficient strategies to improve the optoelectronic and PV performance of PSCs.

Table 3. Summary of the PV performances of recent ternary polymer solar cells (PSCs).

Photoactive Layer	V_{oc} (V)	J_{sc} (mA/cm ²)	FF	PCE (%)	Ref
P3HT:PC ₆₁ BM:CdSe	0.60	8.15	0.62	3.05	[48]
P3HT:PC ₆₁ BM:PCPDTBT	0.62	8.02	0.55	2.8	[49]
P3HT:PC ₆₁ BM:Si-PCPDTBT	0.59	11	0.62	4.0	[50]
P3HT:PC ₆₁ BM:THC8	0.62	11.92	0.53	3.88	[51]
P3HT:PC ₆₁ BM:SiPc	0.58	11.1	0.65	4.13	[52]
P3HT:PC ₆₁ BM:TIPS-pentacene	0.61	10.86	0.62	4.13	[53]
P3HT:PC ₆₁ BM:PCDPP4T	0.53	11.1	0.59	3.5	[54]
P3HT:PC ₆₁ BM:ZnPc	0.62	12.6	0.68	5.3	[55]
P3HT:PCBTDPDP:PC ₆₁ BM	0.64	16.15	0.50	5.28	This work

4. Conclusions

In conclusion, we utilized a compatible low-bandgap polymer, PCBTDPDP into a standard P3HT:PC₆₁BM active system to fabricate efficient ternary PSC with a high PCE of 5.28% as compared to that of the device based on binary P3HT:PC₆₁BM (4.67%). The improvement in the device performance could be mainly attributed to the choice of complementary donor polymer (high mobility, extended absorption), improved exciton migration/dissociation and energy transfer through the judicious incorporation of PCBTDPDP into P3HT:PC₆₁BM. Our results, based on this work, clearly demonstrate the incorporation of a compatible low-bandgap donor into active layer served as an efficient and simple strategy to improve the PV performance of PSCs. Therefore, future work should focus on identifying new kinds of suitable D/A molecules with complementary material properties toward realizing highly efficient ternary-based PSCs.

Author Contributions: G.S. and B.X. involved in methodology evolution, project designing and performed the experiment. V.A.L.R, Q.Q and K.M.R. helped in data interpretation and provided constructive suggestions. S-W.K. guided the project. All authors helped in improving the quality of the manuscript.

Funding: This work was supported in part by National Research Foundation of Korea (NRF) grant funded by the Korea Government (MSIP) (No. NRF 2017R1D1A3B03032042); by the BK21 Plus project funded by the Ministry of Education, Korea (21A20131600011) and by the China Scholarship Council (CSC, No. 201708260004).

Conflicts of Interest: The authors declare no conflict of interest.

References

1. Li, G.; Zhu, R.; Yang, Y. Polymer solar cells. *Nat. Photonics* **2012**, *6*, 153–161. [[CrossRef](#)]
2. Sai-Anand, G.; Gopalan, A.-I.; Lee, K.-P.; Venkatesan, S.; Qiao, Q.; Kang, B.-H.; Lee, S.-W.; Lee, J.-S.; Kang, S.-W. Electrostatic nanoassembly of contact interfacial layer for enhanced photovoltaic performance in polymer solar cells. *Sol. Energy Mater. Sol. Cells* **2016**, *153*, 148–163. [[CrossRef](#)]
3. Liu, Q.; Chen, X.; Hu, W.; Zhang, M.; Ding, L.; Wang, M.; Qiao, Q.; Yang, S. Beyond metal oxides: Introducing low-temperature solution-processed ultrathin layered double hydroxide nanosheets into polymer solar cells toward improved electron transport (solar rrl 2/2019). *Sol. RRL* **2019**, *3*, 1970025. [[CrossRef](#)]
4. Siddiki, M.K.; Venkatesan, S.; Qiao, Q. Nb₂O₅ as a new electron transport layer for double junction polymer solar cells. *Phys. Chem. Chem. Phys.* **2012**, *14*, 4682–4686. [[CrossRef](#)] [[PubMed](#)]
5. Suliman, R.; Mitul, A.F.; Mohammad, L.; Djira, G.; Pan, Y.; Qiao, Q. Modeling of organic solar cell using response surface methodology. *Results Phys.* **2017**, *7*, 2232–2241. [[CrossRef](#)]
6. Mitul, A.F.; Mohammad, L.; Venkatesan, S.; Adhikari, N.; Sigdel, S.; Wang, Q.; Dubey, A.; Khatiwada, D.; Qiao, Q. Low temperature efficient interconnecting layer for tandem polymer solar cells. *Nano Energy* **2015**, *11*, 56–63. [[CrossRef](#)]
7. Venkatesan, S.; Adhikari, N.; Chen, J.; Ngo, E.C.; Dubey, A.; Galipeau, D.W.; Qiao, Q. Interplay of nanoscale domain purity and size on charge transport and recombination dynamics in polymer solar cells. *Nanoscale* **2014**, *6*, 1011–1019. [[CrossRef](#)]
8. Xu, B.; Gopalan, S.-A.; Gopalan, A.-I.; Muthuchamy, N.; Lee, K.-P.; Lee, J.-S.; Jiang, Y.; Lee, S.-W.; Kim, S.-W.; Kim, J.-S.; et al. Functional solid additive modified pedot:Pss as an anode buffer layer for enhanced photovoltaic performance and stability in polymer solar cells. *Sci. Rep.* **2017**, *7*, 45079. [[CrossRef](#)]
9. Kim, J.Y. Effect of solvents on the electrical and morphological characteristics of polymer solar cells. *Polymers* **2019**, *11*, 228. [[CrossRef](#)]
10. Lu, S.; Sun, Y.; Ren, K.; Liu, K.; Wang, Z.; Qu, S. Recent development in ito-free flexible polymer solar cells. *Polymers* **2018**, *10*, 5. [[CrossRef](#)]
11. Zeng, H.; Zhu, X.; Liang, Y.; Guo, X. Interfacial layer engineering for performance enhancement in polymer solar cells. *Polymers* **2015**, *7*, 333–372. [[CrossRef](#)]
12. Roy, J.K.; Kar, S.; Leszczynski, J. Optoelectronic properties of c60 and c70 fullerene derivatives: Designing and evaluating novel candidates for efficient p3ht polymer solar cells. *Materials* **2019**, *12*, 2282. [[CrossRef](#)] [[PubMed](#)]
13. Chen, D.; Nakahara, A.; Wei, D.; Nordlund, D.; Russell, T.P. P3ht/pcbm bulk heterojunction organic photovoltaics: Correlating efficiency and morphology. *Nano Lett.* **2011**, *11*, 561–567. [[CrossRef](#)] [[PubMed](#)]
14. Han, B.; Gopalan, S.-A.; Lee, K.-D.; Kang, B.-H.; Lee, S.-W.; Lee, J.-S.; Kwon, D.-H.; Lee, S.-H.; Kang, S.-W. Preheated solvent exposure on p3ht:Pcbm thin film: A facile strategy to enhance performance in bulk heterojunction photovoltaic cells. *Curr. Appl. Phys.* **2014**, *14*, 1443–1450. [[CrossRef](#)]
15. Kim, Y.; Lim, E. Development of polymer acceptors for organic photovoltaic cells. *Polymers* **2014**, *6*, 382–407. [[CrossRef](#)]
16. Gaspar, H.; Figueira, F.; Pereira, L.; Mendes, A.; Viana, J.C.; Bernardo, G. Recent developments in the optimization of the bulk heterojunction morphology of polymer: Fullerene solar cells. *Materials* **2018**, *11*, 2560. [[CrossRef](#)] [[PubMed](#)]
17. Xu, T.; Yu, L. How to design low bandgap polymers for highly efficient organic solar cells. *Mater. Today* **2014**, *17*, 11–15. [[CrossRef](#)]
18. You, J.; Dou, L.; Hong, Z.; Li, G.; Yang, Y. Recent trends in polymer tandem solar cells research. *Prog. Polym. Sci.* **2013**, *38*, 1909–1928. [[CrossRef](#)]
19. Anantha-Iyengar, G.; Shanmugasundaram, K.; Nallal, M.; Lee, K.-P.; Whitcombe, M.J.; Lakshmi, D.; Sai-Anand, G. Functionalized conjugated polymers for sensing and molecular imprinting applications. *Prog. Polym. Sci.* **2019**, *88*, 1–129. [[CrossRef](#)]

20. Yang, M.H.; Jin, H.C.; Kim, J.H.; Chang, D.W. Synthesis of cyano-substituted conjugated polymers for photovoltaic applications. *Polymers* **2019**, *11*, 746. [[CrossRef](#)]
21. Mitul, A.F.; Sarker, J.; Adhikari, N.; Mohammad, L.; Wang, Q.; Khatiwada, D.; Qiao, Q. Efficient csf interlayer for high and low bandgap polymer solar cell. *AIP Adv.* **2018**, *8*, 025018. [[CrossRef](#)]
22. Li, J.; Liang, Z.; Peng, Y.; Lv, J.; Ma, X.; Wang, Y.; Xia, Y. 36% enhanced efficiency of ternary organic solar cells by doping a nt-based polymer as an electron-cascade donor. *Polymers* **2018**, *10*, 703. [[CrossRef](#)]
23. Hou, W.; Xiao, Y.; Han, G.; Lin, J.-Y. The applications of polymers in solar cells: A review. *Polymers* **2019**, *11*, 143. [[CrossRef](#)] [[PubMed](#)]
24. Lu, L.; Chen, W.; Xu, T.; Yu, L. High-performance ternary blend polymer solar cells involving both energy transfer and hole relay processes. *Nat. Commun.* **2015**, *6*, 7327. [[CrossRef](#)] [[PubMed](#)]
25. Zhang, S.; Zuo, L.; Chen, J.; Zhang, Z.; Mai, J.; Lau, T.-K.; Lu, X.; Shi, M.; Chen, H. Improved photon-to-electron response of ternary blend organic solar cells with a low band gap polymer sensitizer and interfacial modification. *J. Mater. Chem. A* **2016**, *4*, 1702–1707. [[CrossRef](#)]
26. Shen, L.; Yu, W.; Long, Y.; Guo, W.; Meng, F.; Ruan, S.; Chen, W. Performance improvement of low-band-gap polymer solar cells by optical microcavity effect. *IEEE Electron Device Lett.* **2013**, *34*, 87–89. [[CrossRef](#)]
27. Kim, H.D.; Shimizu, R.; Ohkita, H. Ternary blend polymer solar cells based on wide-bandgap polymer pdcbt and low-bandgap polymer ptb7-th. *Chem. Lett.* **2018**, *47*, 1059–1062. [[CrossRef](#)]
28. Yang, P.; Zhou, X.; Cao, G.; Luscombe, C.K. P3ht:Pcbm polymer solar cells with tio2 nanotube aggregates in the active layer. *J. Mater. Chem.* **2010**, *20*, 2612–2616. [[CrossRef](#)]
29. Zou, Y.; Gendron, D.; Badrou-Aïch, R.; Najari, A.; Tao, Y.; Leclerc, M. A high-mobility low-bandgap poly(2,7-carbazole) derivative for photovoltaic applications. *Macromolecules* **2009**, *42*, 2891–2894. [[CrossRef](#)]
30. Cai, B.; Xing, Y.; Yang, Z.; Zhang, W.-H.; Qiu, J. High performance hybrid solar cells sensitized by organolead halide perovskites. *Energy Environ. Sci.* **2013**, *6*, 1480–1485. [[CrossRef](#)]
31. Cheun, H.; Kim, J.; Zhou, Y.; Fang, Y.; Dindar, A.; Shim, J.; Fuentes-Hernandez, C.; Sandhage, K.H.; Kippelen, B. Inverted polymer solar cells with amorphous indium zinc oxide as the electron-collecting electrode. *Opt. Express* **2010**, *18*, A506–A512. [[CrossRef](#)] [[PubMed](#)]
32. Zou, Y.; Gendron, D.; Neagu-Plesu, R.; Leclerc, M. Synthesis and characterization of new low-bandgap diketopyrrolopyrrole-based copolymers. *Macromolecules* **2009**, *42*, 6361–6365. [[CrossRef](#)]
33. Gopalan, S.-A.; Gopalan, A.-I.; Vinu, A.; Lee, K.-P.; Kang, S.-W. A new optical-electrical integrated buffer layer design based on gold nanoparticles tethered thiol containing sulfonated polyaniline towards enhancement of solar cell performance. *Sol. Energy Mater. Solar Cells* **2018**, *174*, 112–123. [[CrossRef](#)]
34. Gopalan, S.-A.; Seo, M.-H.; Anantha-Iyengar, G.; Han, B.; Lee, S.-W.; Kwon, D.-H.; Lee, S.-H.; Kang, S.-W. Mild wetting poor solvent induced hydrogen bonding interactions for improved performance in bulk heterojunction solar cells. *J. Mater. Chem. A* **2014**, *2*, 2174–2186. [[CrossRef](#)]
35. Sai-Anand, G.; Gopalan, A.-I.; Lee, K.-P.; Venkatesan, S.; Kang, B.-H.; Lee, S.-W.; Lee, J.-S.; Qiao, Q.; Kwon, D.-H.; Kang, S.-W. A futuristic strategy to influence the solar cell performance using fixed and mobile dopants incorporated sulfonated polyaniline based buffer layer. *Sol. Energy Mater. Solar Cells* **2015**, *141*, 275–290. [[CrossRef](#)]
36. Xu, B.; Sai-Anand, G.; Jeong, H.-M.; Kim, S.-W.; Kim, J.-S.; Kwon, J.-B.; Kang, S.-W. Improving air-stability and performance of bulk heterojunction polymer solar cells using solvent engineered hole selective interlayer. *Materials* **2018**, *11*, 1143. [[CrossRef](#)] [[PubMed](#)]
37. Xu, B.; Sai-Anand, G.; Unni, G.E.; Jeong, H.-M.; Kim, J.-S.; Kim, S.-W.; Kwon, J.-B.; Bae, J.-H.; Kang, S.-W. Pyridine-based additive optimized p3ht:Pc61bm nanomorphology for improved performance and stability in polymer solar cells. *Appl. Surf. Sci.* **2019**, *484*, 825–834. [[CrossRef](#)]
38. Fan, P.; Zheng, Y.; Zheng, D.; Yu, J. Improved efficiency of bulk heterojunction polymer solar cells by doping with iridium complex. *Mater. Letters* **2017**, *186*, 161–164. [[CrossRef](#)]
39. Xu, W.-L.; Wu, B.; Zheng, F.; Yang, X.-Y.; Jin, H.-D.; Zhu, F.; Hao, X.-T. Förster resonance energy transfer and energy cascade in broadband photodetectors with ternary polymer bulk heterojunction. *J. Phys. Chem. C* **2015**, *119*, 21913–21920. [[CrossRef](#)]
40. Zhang, C.; Zhang, P.; Xu, X.; Dang, Y.; Chen, X.; Kang, B. Effect of alq3 layer for power-conversion-efficiency enhancement of polymer solar cells. *Mater. Letters* **2016**, *164*, 591–594. [[CrossRef](#)]
41. Xu, B.; Sai-Anand, G.; Gopalan, A.-I.; Qiao, Q.; Kang, S.-W. Improving photovoltaic properties of p3ht:Ic60ba through the incorporation of small molecules. *Polymers* **2018**, *10*, 121. [[CrossRef](#)] [[PubMed](#)]

42. Sai-Anand, G.; Dubey, A.; Gopalan, A.-I.; Venkatesan, S.; Ruban, S.; Reza, K.M.; Choi, J.; Lakhi, K.S.; Xu, B.; Qiao, Q.; et al. Additive assisted morphological optimization of photoactive layer in polymer solar cells. *Sol. Energy Mater. Solar Cells* **2018**, *182*, 246–254. [[CrossRef](#)]
43. Shen, W.; Chen, W.; Zhu, D.; Zhang, J.; Xu, X.; Jiang, H.; Wang, T.; Wang, E.; Yang, R. High-performance ternary polymer solar cells from a structurally similar polymer alloy. *J. Mater. Chem. A* **2017**, *5*, 12400–12406. [[CrossRef](#)]
44. Mai, R.; Wu, X.; Jiang, Y.; Meng, Y.; Liu, B.; Hu, X.; Roncali, J.; Zhou, G.; Liu, J.-M.; Kempa, K.; et al. An efficient multi-functional material based on polyether-substituted indolocarbazole for perovskite solar cells and solution-processed non-doped oleds. *J. Mater. Chem. A* **2019**, *7*, 1539–1547. [[CrossRef](#)]
45. Luo, D.; Chen, Q.; Liu, B.; Qiu, Y. Emergence of flexible white organic light-emitting diodes. *Polymers* **2019**, *11*, 384. [[CrossRef](#)] [[PubMed](#)]
46. Ouyang, L.; Musumeci, C.; Jafari, M.J.; Ederth, T.; Inganäs, O. Imaging the phase separation between pedot and polyelectrolytes during processing of highly conductive pedot:Pss films. *ACS Appl. Mater. Interfaces* **2015**, *7*, 19764–19773. [[CrossRef](#)] [[PubMed](#)]
47. Mohapatra, A.A.; Kim, V.; Puttaraju, B.; Sadhanala, A.; Jiao, X.; McNeill, C.R.; Friend, R.H.; Patil, S. Förster resonance energy transfer drives higher efficiency in ternary blend organic solar cells. *ACS Appl. Mater. Interfaces* **2018**, *1*, 4874–4882. [[CrossRef](#)]
48. Fu, H.; Choi, M.; Luan, W.; Kim, Y.-S.; Tu, S.-T. Hybrid solar cells with an inverted structure: Nanodots incorporated ternary system. *Solid-State Electron.* **2012**, *69*, 50–54. [[CrossRef](#)]
49. Koppe, M.; Egelhaaf, H.-J.; Dennler, G.; Scharber, M.C.; Brabec, C.J.; Schilinsky, P.; Hoth, C.N. Near ir sensitization of organic bulk heterojunction solar cells: Towards optimization of the spectral response of organic solar cells. *Adv. Funct. Mater.* **2010**, *20*, 338–346. [[CrossRef](#)]
50. Ameri, T.; Min, J.; Li, N.; Machui, F.; Baran, D.; Forster, M.; Schottler, K.J.; Dolfen, D.; Scherf, U.; Brabec, C.J. Performance enhancement of the p3ht/pcbm solar cells through nir sensitization using a small-bandgap polymer. *Adv. Funct. Mater.* **2012**, *2*, 1198–1202. [[CrossRef](#)]
51. Chi, C.-Y.; Chen, M.-C.; Liaw, D.-J.; Wu, H.-Y.; Huang, Y.-C.; Tai, Y. A bifunctional copolymer additive to utilize photoenergy transfer and to improve hole mobility for organic ternary bulk-heterojunction solar cell. *ACS Appl. Mater. Interfaces* **2014**, *6*, 12119–12125. [[CrossRef](#)] [[PubMed](#)]
52. Honda, S.; Ohkita, H.; Benten, H.; Ito, S. Selective dye loading at the heterojunction in polymer/fullerene solar cells. *Adv. Funct. Mater.* **2011**, *1*, 588–598. [[CrossRef](#)]
53. Wang, H.; Wang, X.; Fan, P.; Yang, X.; Yu, J. Enhanced power conversion efficiency of p3ht: pc71bm bulk heterojunction polymer solar cells by doping a high-mobility small organic molecule. *Int. J. Photoenergy* **2015**, *2015*, 8. [[CrossRef](#)]
54. Wang, Y.; Chen, J.; Kim, H.D.; Wang, B.; Iriguchi, R.; Ohkita, H. Ternary blend solar cells based on a conjugated polymer with diketopyrrolopyrrole and carbazole units. *Front. Energy Res.* **2018**, *6*. [[CrossRef](#)]
55. Kadem, B.; Hassan, A.; Göksel, M.; Basova, T.; Şenocak, A.; Demirbaş, E.; Durmuş, M. High performance ternary solar cells based on p3ht:Pcbm and znpc-hybrids. *RSC Adv.* **2016**, *6*, 93453–93462. [[CrossRef](#)]

